Registration of the quantum state of a single photon to create a satellite quantum network

Registration of the quantum state of a single photon to create a satellite quantum network

V L Kurochkin[1,3,4], A V Khmelev[1,2], I V Petrov[1,2], A V Miller[3], A A Feimov[3], V F Mayboroda[3], M Y Balanov[3,4], V V Krushinsky[5], A A Popov[6] and Y V Kurochkin[1,2,3,4]

[1] Russian Quantum Center, Moscow, Russia
[2] MIPT, Dolgoprudny, Russia
[3] QRate, Moscow, Russia
[4] NTI Center for Quantum Communications, NUST MISIS, Moscow, Russia
[5] Laboratory of Astrochemistry and Extraterrestrial Physics, UrFU, Ekaterinburg, Russia
[6] Kourovka observatory, UrFU, Ekaterinburg, Russia

E-mail: v.kurochkin@rqc.ru

Abstract. Artificial satellites employed as trusted nodes can increase the distance between two parties to establish quantum key distribution (QKD), unlike fiber based communication lines that are limited up to a few hundred kilometers. This report summarises our progress on a ground receiver for satellite QKD and its tracking receiving system (TRS). The authors demonstrate the operation of the TRS in practice and achieve standard tracking error of 1.4 μrad observing four satellites over 80% of the time they were available. The optical signal, which was the sunlight reflected of low Earth orbit satellites, was attenuated to a single photon level and was detected effectively using avalanche single photon detectors. The authors have thus proved that the developed system is capable of stable reception of quantum signal from a satellite.

1. Introduction

Nowadays quantum cryptography is considered the only data encryption method which reliability is not based on the computation complexity of its algorithms but physical principles. Charles Bennett and Gilles Brassard were the first who introduced the idea of quantum key distribution (QKD) and proposed the first quantum cryptography protocol [1] in 1984. Five years later, in 1989, the first quantum key distribution experiment was carried out [2]. The world first quantum key distribution network was built in the city of Boston (USA) in 2002 [3]. Later quantum key distribution networks were built in Austria [4], Switzerland [5], China [6, 7], Japan [8] and USA [9]. Building a global network using only existing fiber-optic cable infrastructure seems non-practical because of high attenuation of signal in optical fiber.

The use of artificial satellites as trusted nodes is thus the only way to establish a global quantum key distribution network. Galassia, which is a nanosatellite developed by the National University of Singapore, was launched into its orbit in 2015. One of the payloads of Galassia was a source of polarization-entangled photons and their analyzer. Such equipment demonstrated its robust operation despite high exposure of space radiation [10]. In Japan, the team of the National Institute of Information and Communications Technology has demonstrated the transmission of the "pseudo quantum" signal from SOCRATES microsatellite to the ground station. The

intensity of optical signal was a few orders of magnitude larger than that required to ensure secure communication. However, the approach that solved some issues such as clock synchronization and polarization reference frame was a major step forward in this field [11]. Currently the leader in satellite quantum communications is China, where researchers have launched a medium-sized satellite, known as Mozi or Micius, and demonstrated for the first time satellite-to-ground quantum key distribution [12].

Despite the progress made, satellite quantum communications still have great potential for further improvement. Thus, there is a challenge to develop the concept of a global quantum key distribution network based on satellite constellations with the possibility of integration into existing fiber-optic network systems. To make the technology of satellite quantum communications practical, it is also necessary to reduce the size and cost of dedicated satellites significantly. To date, the authors have developed a system for quantum key distribution, with a rate of information pulses more than 300 MHz, and performed a QKD between two remote ground-based users [13].

In the present article, in section II, we show schematic of the ground receiver developed for quantum key distribution with a satellite and consider the procedure challenges. In section III, we present our tracking receiving system, which is a part of the ground receiver, and describe its operational principle. In section IV, the results of satellites tracking are presented.

2. Ground receiver for free-space QKD with a satellite

Polarization encoding of photons transmitted from the satellite is well suited to free-space quantum key distribution [14]. It is assumed that we can decode a quantum signal prepared in one of the four states, according to the BB84 protocol. Thus, the horizontal and vertical states in the Z basis or the diagonal and anti-diagonal in the X basis correspond to bit values 0 and 1 for each basis.

Figure 1 displays a developed scheme of the satellite quantum signals receiver with passive basis selection. Here, the 'red' (850 nm) and 'green' (532 nm) beams are reflected of the hand adjustable mirrors (M1, M2) and fast steering mirror (FSM) and focus in front of the dichroic

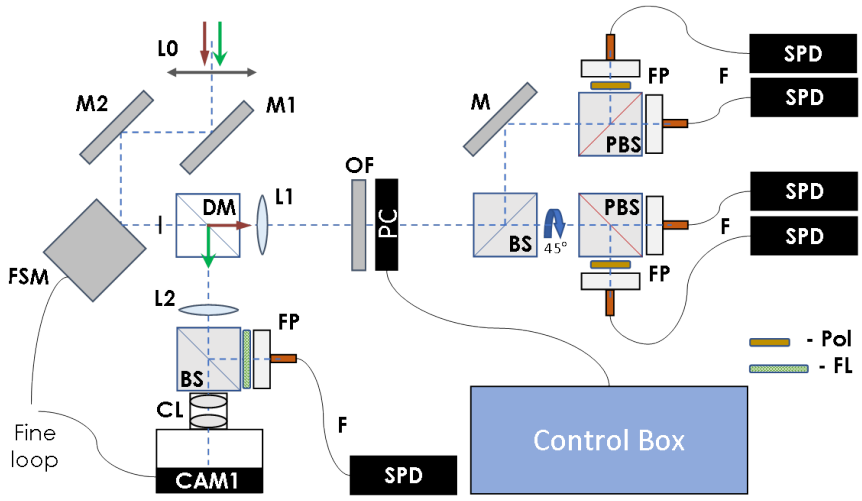

Figure 1. Schematic of the ground receiver for polarization decoding. Hand adjustable mirrors (M1, M2, M); fast steering mirror (FSM); dichroic mirror (DM); lenses (L0, L1, L2); 50:50 beam splitter (BS); spectral filter (FL, 532 nm); fast camera (CAM1); camera lens (CL); optical filters (OF, 850 nm); polarization controller (PC); polarization beam splitter (PBS); polarizer (Pol); fiber port collimators (FP); multimode fiber (F); avalanche single photon detector (SPD).

mirror (DM) by a lens (L0). These beams split into two channels: a signal part (850 nm) and a synchronization-stabilization part (532 nm), that are collimated by the lenses (L1, L2). The 'green arrow' channel splits on 50:50 beam splitter (BS) into a synchronization part, which has a filter (FL, 532 nm), and a stabilization part, which consists of the fast camera (CAM, 100 Hz) and the camera lens (CL). The signal channel has a standard BB84 decoder, where rotation at 45° in the X basis is performed mechanically and the polarization beam splitters (PBS) have an additional polarizers (Pol) in the reflected arm. Eventually, the beams go through fiber port collimators (FP, 4.6 mm F.L. for 850 nm; 7.5 mm F.L. for 532 nm) coupled with multimode fiber (F), and optical signals are detected by avalanche single photon detectors (SPD) and are transmitted to the control box.

To detect photons effectively, the receiver contains some special modules in addition to the decoder of the quantum states. In particular, it is a polarization controller (PC), which is intended to offset the change in polarization caused mainly by satellite rotation. Also, there are spectral optical filters (OF) and a time filtering system that are used to maintain signal-to-noise ratio at the desired level, as well as the fine control loop (FSM, CAM1) which is intended to suppress the beam deflection.

To achieve low loss of the quantum signals sent from a satellite, the ground receiver is used in combination with a telescope, in place of the focusing lens L0. That provides a high ratio of the collected light to the light spot on the ground that raises the quantum bitrate. At the same time, a wider aperture of the receiver requires the larger focal length and increases of the amplitude of beam wandering. Hence, the scheme has a modified acquisition, pointing and tracking system (APT) to maintain stable optical signal detection in the fiber. In the present work, we developed a modified receiver that was implemented as an independent part of the ground receiver and tested in an astronomical observatory.

3. Experimental setup

The schematic of our tracking receiving system, which is designed to collect arbitrary single photons reflected of low Earth orbit (LEO) satellites, is shown in figure 2a. The TRS mainly consists of a mounted telescope, a guide scope, a receiver module, and a control box. The 1.2-meter Cassegrain system telescope, used with two-axis altazimuth mount, has a Nasmyth focal length f_T of 12 m and, in pair with the guide scope, performs coarse tracking of satellites. The receiver module, which is designed for optical signal detection, is mounted behind the focal plane of the telescope and offsets residual beam deflection. As shown in Fig.2a, all incoming light rays are reflected by FSM and focused at the telescope focal plane, which coincides with the focal planes of lenses L1 and L2 with focal lengths of 40 and 75 mm, respectively. At the beam splitter (BS) the beam is divided into two parts. The first part is focused on the fast camera (640×640 px) used to measure beam deflection of the optical axis. The second one is focused on the core of the optical fiber (F) by the lens into the fiber port (FP).

There are two parameters of the optical fiber that limit the maximum allowable deviation $\delta\varphi$ of the telescope from the exact direction at the satellite. It is a numerical aperture NA and core diameter CD, which are equal to 0.22 and 105 μm in our experiments. Taking the distance between L1 and FP lenses equals to $l = 220$ mm, it is straightforward to deduce the constraint on the magnitude of telescope deviation.

$$\delta\varphi \leq \frac{f_{L1} \cdot f_{FP}}{(l - f_{FP} - f_{L1}) \cdot f_T} \cdot NA = 33\,\mu rad \tag{1}$$

$$\delta\varphi \leq \frac{CD}{2} \frac{f_{L1}}{f_{FP} \cdot f_T} = 24\,\mu rad \tag{2}$$

Angular size γ of the LEO satellite is estimated at 10 μrad, with its image on the CAM1 of about 40 μm, according to Eq.3, where f_{CL} and f_{L2} are the focal lengths of CL and L2 lenses.

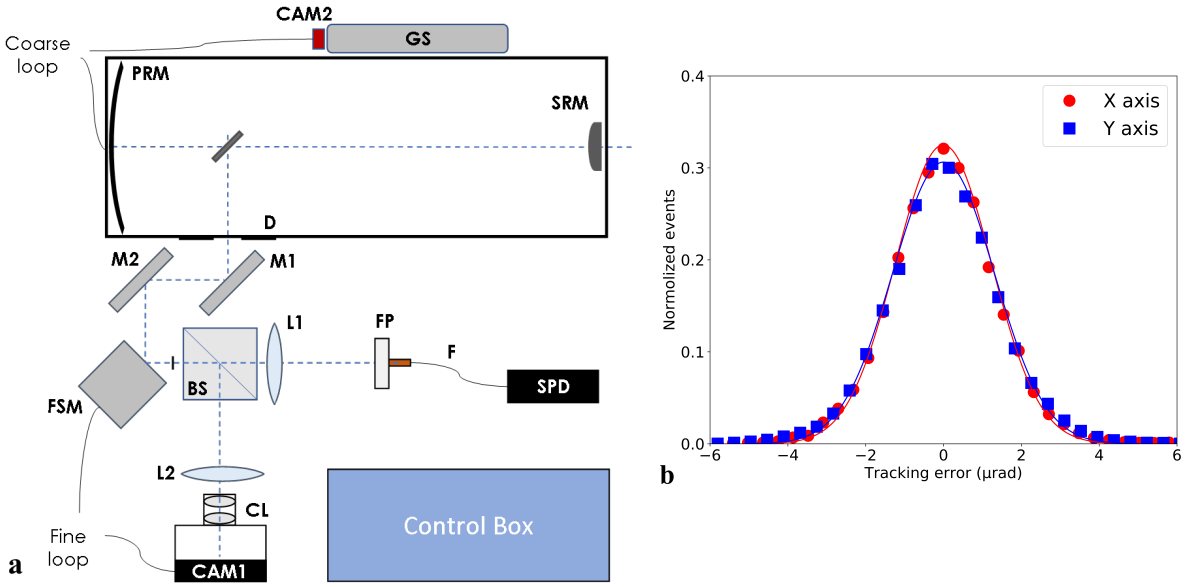

Figure 2. The experiments on satellites tracking. **a**, Schematic of our experimental tracking receiving system. 1.2m-aperture Cassegrain telescope (12 m F.L.); primary mirror (PRM); secondary mirror (SRM); diaphragm (D); guide scope (GS, 400 mm F.L.; aperture of 66 mm); large field-of-view guide camera (CAM2, 5 Hz); hand adjustable mirrors (M1, M2); fast steering mirror (FSM); beam splitter (BS, 400-700 nm); lenses (L1, 40 mm F.L.; L2, 75 mm F.L.); fast stabilization camera (CAM1, 100 Hz); camera lens (CL, 25 mm F.L.); fiber port (FP, 7.5 mm F.L.); 105μm-multimode fiber (F) with an optical fiber attenuator; avalanche single photon detector (SPD); control box. **b**, Distribution of an object 16612 tracking errors along the X and Y axes extracted from the real-time images recorded with the fast camera.

In our experiments, the typical value of an image spot equals 44 μm that is consistent with the above estimate.

$$S = \gamma \cdot \frac{f_T}{f_{L2}} \cdot f_{CL} \tag{3}$$

Using Eq.1, Eq.2, and considering the angular size of the satellite, the maximum tracking error $\delta\varphi$ should be less than $\pm 20\,\mu$rad.

Hence, the TRS has a cascaded two-stage system of acquisition and tracking the reflected sunlight, and the control box containing electronic units manages both the coarse-tracking and the fine-tracking loops. It is worth mentioning that the fine feedback loop and the coarse feedback loop operate independently.

The first stage of this system is the coarse control loop which tracks the satellite orbit predicted by two-line element sets (TLE). In advance, the control box gets the current coordinates of telescope and TLE data and then calculates the position of a satellite (Azimuth, Elevation) using a simplified general perturbations model (SGP4). So, during the tracking, the guide camera (FOV of 1° x 1°, frame rate of 5 Hz) on the telescope captures the image of the satellite, defines the coordinates of the spot on the frames, and the control box computes the position error (Az Error; El Error) of the telescope. Based on the result, one calculates proportional integral derivative (PID) correction for the two-axis telescope mount and finally sets the new rate of the telescope axes movement. Thus, the coarse control loop provides $\pm 400\,\mu$rad of tracking error obtained from preliminary experimental data. Accordingly, this first stage with a large field of

view allows us to apply fine feedback control of the receiver module with a more precise correction of the beam.

The second stage is the fine-control loop, including an FSM driven by a voice-coil (working range of ±26.2 mrad) and a CCD camera (0.9 mrad×0.9 mrad, frame rate of 100 Hz). As stated above, the focal plane of the telescope coincides with those of lenses L1 and L2. FSM is placed somewhat before it so that the distance x from the mirror to the focal plane is equal to 91.5 mm. Once the narrow field-of-view camera (CAM1) captures the picture of the satellite, the control system determines the center of the image, calculates the PID correction signal and applies it to FSM.

It is easy to prove that the angle that FSM needs to be rotated by to compensate a beam deviation of $\delta\theta$ is equal to

$$\delta\alpha = \frac{1}{2}\frac{(f_T - x)}{x} \cdot \delta\theta, \tag{4}$$

and since $x \ll f_T$ in our case, it can be rewritten as

$$\delta\alpha = \frac{1}{2}\frac{f_T}{x} \cdot \delta\theta. \tag{5}$$

Using Eq.5, one can calculate the corresponding beam deviation $\delta\theta$ that could be compensated by the mirror with its maximum working range of the ±26.2 mrad and located at the distance 91.5 mm, which would be about ±400 μrad. Since the maximum deflection angle provided by the first stage of the telescoping adjustment does not exceed this value, the system should operate successfully. That was confirmed by achieving the experimental tracking error $3\sigma = 4.2\,\mu$rad (Fig.2b).

4. Results of the experiments

The experiments were carried out at the Kourovka Astronomical Observatory, which is located near Sloboda village (57° 02′ 12.1″ N, 59° 32′ 50.18″ E, an altitude of 290 m). The results of satellite tracking obtained on the night of September 13-14 are presented in Table 1. During that night we observed and tracked four different satellites. The duration of sustainable tracking determined as the time while the first stage was able to keep beam deflection within 400 μrad, was equal, on average, 160 sec. The second stage, which provides fine compensation, was, on average, working over 80% of this time. The best results obtained during satellite tracking were 250 sec and 100%, for the first and second stages respectively. The quality of fine compensation was evaluated on the basis of two parameters measured during tracking. First of all, we measured the single photon count rate for attenuated optical signal collected into the fiber. We watched a star with a similar apparent magnitude (3.67) beforehand so that we were able to calculate the expected max count rate for all the satellites. The corresponding values are presented in the bottom row of Table 1. The stable tracking of satellite ID36089 (satellite catalog number) was interrupted for a few seconds because the satellite passed too close to a bright star. Only the time before the interruption is shown in Table 1, whereas the time after the interruption was 116 sec, thus totaling 219 sec.

Also, we watched the beam deviation using the camera (CAM1). To obtain the tracking error from the camera captures, we calculated angle with Eq.3, considered a linear displacement of 1 pixel that equals 5.5 μm, and got 1.42 μrad per pixel coefficient. After the camera captured a satellite image, the algorithm started to send the beam in a conditional center and kept it there with an accuracy of about ±1px, which corresponds to a standard angular deviation of 1.4 μrad. Normalized statistics of deviated beam events collected during the experiment of tracking object ID16612 is shown in figure 2b. It is calculated from angular beam deflections detected by the fine camera and normalized by the total count in each 0.25 μrad-sized bin.

Table 1. The results of satellite tracking obtained at Kourovka Astronomical Observatory on the night of 13-14 September 2019. Satellite tracking begins once the elevation angle becomes equal to 20°. Apparent magnitudes are presented for the middle of coarse tracking time.

Satellite Catalog Number	11511	10967	36089	16612
Satellite tracking start time (UTC)	13.09 23:46:46	14.09 0:04:04	14.09 0:19:42	14.09 0:46:14
Total tracking time (elevation angle $\geq 20°$), sec	410	400	350	300
The time of sustainable tracking, sec	90	125	180	250
Max beam deviation during sustainable tracking, μrad	270	330	280	300
The time while the beam was being collected into the fiber, sec	69	99	103	250
Apparent magnitude	3.5	2.9	3.5	3.4
Max actual and expected count rates, counts/sec	$4 \cdot 10^4$ $(1.2 \cdot 10^5)$	$1.3 \cdot 10^5$ $(2.0 \cdot 10^5)$	$3.5 \cdot 10^5$ $(1.2 \cdot 10^5)$	$1.7 \cdot 10^5$ $(1.4 \cdot 10^5)$

The results of tracking experiment of satellite ID16612 are presented in Fig.3 as an example of the time evolution of both the light signal and the beam angular deviation with and without fine loop operating. Here we also observe PID signal disturbance between 125 and 175 seconds, which could be caused by signal obscuration by clouds we encountered while tracking the satellite.

5. Conclusions

In this work, the implementation of the ground receiver employing the BB84 quantum key distribution protocol is presented. The ground receiver of polarization encoded quantum states includes the wide-aperture telescope for effective reception of the dual-wavelength, two-channel light signal, the guide scope and the receiver module. The receiver module is responsible for decoding BB84-states and for precise tracking of low Earth orbit satellites. The two-stage auto-tracking system, which appears when using a pre-calculated satellite trajectory, is described in detail. The estimation of the acceptable tracking error for our modified setup (TRS) showed that to successful holding of incoming beams on the core of the fiber during the entire time of satellite observation can be achieved with tracking error of $< 20\,\mu$rad. However, during the test on collecting the sunlight reflected of satellites, the receiver demonstrates tracking with the standard deviation at a level of $1.4\,\mu$rad within 80% of coarse tracking time, on average. This should be more than enough to distribute quantum key between our ground receiver and a satellite successfully in the future. It is worth mentioning that our feedback system shows sustainable tracking of the satellite only under good weather conditions. There are decreases of signal or even operating failures in the presence of both clouds and fog. Moreover, cloudiness

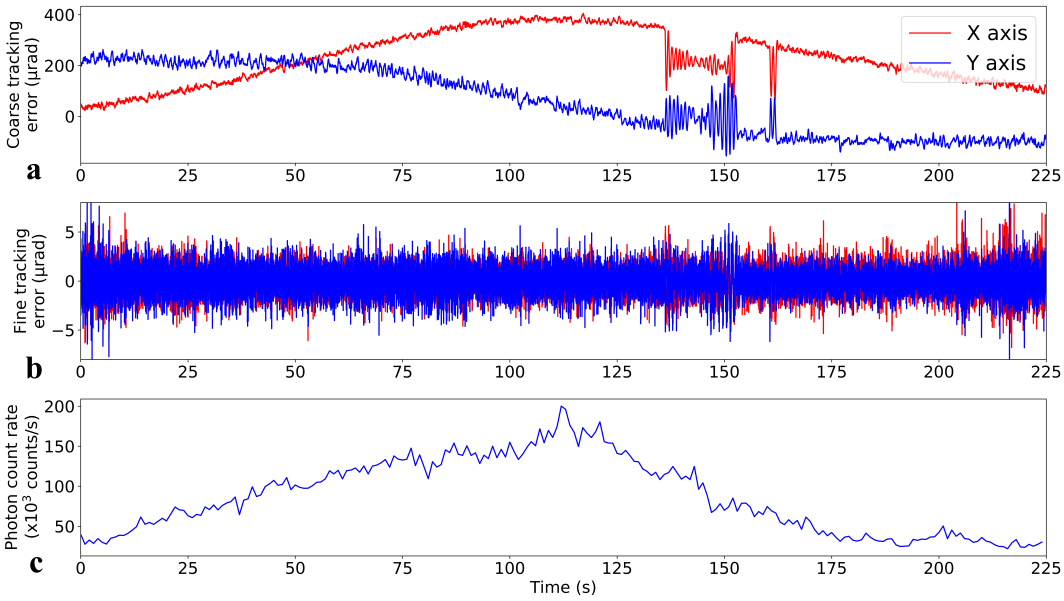

Figure 3. The tracking experiment of the satellite (NORAD ID 16612). **a**, Calculated an angular deviation of incoming light rays according to a PID signal for the FSM controller. **b**, Angular deviation extracted from the fast camera after fine control loop adjusting. **c**, Single-photon counts are recorded by the SPD in parallel with the PID and camera signals.

blocks satellite quantum communication in general since the photons used to transmit quantum states have a similar wavelength to that scattered by clouds. We also observed that bright starts might impose one more restriction on the system. If a satellite passes too close to a star with a greater brightness, the algorithm mistakes the star for the satellite, and the tracking is interrupted. Although the probability of such events is not too high, they should be kept in mind for future development. However, the authors have demonstrated that their tracking receiving system is potentially capable of distributing quantum keys between a satellite and the ground receiving station that form a subsystem of a quantum satellite network.

Acknowledgments

This work is supported by Russian Science Foundation (grant No. 17-71-20146).

References

[1] Bennett C H and Brassard G 1984 *Proc. Int. Conf. on Computers, Systems & Signal Processing* (Bangalore) pp 175–9
[2] Bennett C H, Bessette F, Brassard G, Salvail L and Smolin J 1992 Experimental quantum cryptography *J. Cryptol.* **5** 3-28
[3] Elliott C 2002 Building the quantum network *New J. Phys.* **4** 46
[4] Poppe A, Peev M and Maurhart O 2008 Outline of the SECOQC quantum-key-distribution network in Vienna *Int. J. Quantum Inf.* **6** 209-18
[5] Stucki D *et al* 2011 Long-term performance of the SwissQuantum quantum key distribution network in a field environment *New J. Phys.* **13** 123001
[6] Xu F X *et al* 2009 Field experiment on a robust hierarchical metropolitan quantum cryptography network *Chin. Sci. Bull.* **54** 2991-7
[7] Wang S *et al* 2010 Field test of the wavelength-saving quantum key distribution network *Opt. Lett.* **35** 2454-6
[8] Sasaki M *et al* 2011 Field test of quantum key distribution in the Tokyo QKD network *Opt.Express* **19** 10387-409

[9] Hughes R J *et al* 2013 Network-centric quantum communications with application to critical infrastructure protection *Proc. of QCRYPT 2013* (Waterloo)
[10] Tang Z *et al* 2016 Generation and analysis of correlated pairs of photons on board a nanosatellite *Phys. Rev.* Appl. **5** 054022
[11] Takenaka H *et al* 2017 Satellite-to-ground quantum communication using a 50-kg-class micro-satellite *Nat. Photonics* **11** 502-8
[12] Liao S K *et al* 2017 Satellite-to-ground quantum key distribution *Nature* **549** 43-7
[13] Kurochkin V L, Miller A V, Rodimin V E, Vorobey S S, Balanov M Y and Kurochkin Y V 2019 Quantum key distribution for ultra-long distances based on microsatellites *AIP Conf. Proc.* **2069** 03003
[14] Bedington R, Arrazola J M and Ling A 2017 Progress in satellite quantum key distribution *NPJ Quantum Inf.* **3** 30